

Journal of Materials Chemistry B

Accepted Manuscript



This is an *Accepted Manuscript*, which has been through the Royal Society of Chemistry peer review process and has been accepted for publication.

Accepted Manuscripts are published online shortly after acceptance, before technical editing, formatting and proof reading. Using this free service, authors can make their results available to the community, in citable form, before we publish the edited article. We will replace this *Accepted Manuscript* with the edited and formatted *Advance Article* as soon as it is available.

You can find more information about *Accepted Manuscripts* in the [Information for Authors](#).

Please note that technical editing may introduce minor changes to the text and/or graphics, which may alter content. The journal's standard [Terms & Conditions](#) and the [Ethical guidelines](#) still apply. In no event shall the Royal Society of Chemistry be held responsible for any errors or omissions in this *Accepted Manuscript* or any consequences arising from the use of any information it contains.



Direct cellular organization with ring-shaped composite polymer and glass substrates for urethral sphincter tissue engineering

Wenqiang Du, Jianfeng Chen, Huan Li, Gang Zhao,* Guangli Liu, Wulin Zhu, Dong Wu and Jiaru Chu

Received 00th January 20xx,
Accepted 00th January 20xx

DOI: 10.1039/x0xx00000x

www.rsc.org/

Although fundamental efforts have been made to engineer circular smooth muscle layers in vitro, engineering structured skeletal muscle tissue equivalents acting as sphincters remains to be investigated. Groove patterned substrates made of homogeneous material usually leads to cell monolayers instead of patterned cell sheets while patterned matrix failed to generate circular myotubes because cell chirality blocks the end-to-end cellular sequence corresponding to pattern directions. In this paper, we proposed concentric circular and elliptical microgroove patterned substrates with glass as grooves and polymer as ridges to direct ring-shaped myoblast patterns and maximize cell alignment with respect to constraints directions, which is essential for circular myotubes generation towards sphincter tissue engineering. Our results showed that our substrates direct myoblasts to proliferate in and orient with directions of glass grooves, leading to higher cell alignment degree than homogeneous substrate can achieve. We also found that cell alignment degree depends on dimension and parallelism other than curvature of the constraint. On the basis of these findings, we proposed finite element models that quantitatively account for our experimental data and emphasized the role intercellular forces played in cell alignment modulation. These results suggest that narrow curved constraints with parallel boundaries can favourably maximize myoblast alignment and facilitate myogenic differentiation regardless of constraint curvature, which will underpin the design of substrates and scaffolds for urethral sphincter or other hollow tissue engineering applications.

1 Introduction 22 and so forth is permanent.^{1,2} Millions of people are affected
23 and billions US dollars are cost annually worldwide. The trends
24 that urethral skeletal muscle reduces rapidly with age
25 increasing makes SUI a major issue to be concerned.
26 Treatments of SUI through related muscle training,
27 pharmaceutical injection, medical devices installation and
28 surgery only have limited effects and are probably associated
29 with complications. Stem cell therapy for SUI has recently
30 provided a promising options for SUI treatment in vivo. But the
31 unhealthy microenvironments inside SUI patients are possibly
32 unable to provide sufficient differentiation and consequential
33 cellular architectural organization cues for urethral sphincter
34 regeneration.³ Therefore, it is crucial to engineer circular ring-
35 shaped external urethral sphincter in vitro.⁴
36 In order to restore circular external urethral sphincter in vitro,
37 both cell patterns and cell alignment have to be engineered.
38 Engineering ring-shaped cell patterns and maximizing cell
39 alignment corresponded to cell patterns are vital to circular
40 myotubes generation and important stages of urethral
41 sphincter engineering. Higher degree of cell alignment
42 corresponded to ring-shaped cell patterns means more end-to-
43 end cellular sequence, which can facilitate myoblasts fusion
44 towards ring-shaped myotubes generation. The state-of-the-
45 art approaches to engineer cell patterns in two dimensions are
46 usually accompanied with oriented cells. These approaches
47 mainly include chemical cues such as surface matrix
48 patterning.⁵⁻⁹ However, physical cues such as topographical
49 and mechanical simulations have been demonstrated to play a

Department of Precision Machinery and Precision Instrumentation, University of
Science and Technology of China, Hefei 230027, China
Email: fvc@ustc.edu.cn

Electronic Supplementary Information (ESI) available: [details of any
supplementary information available should be included here]. See
DOI: 10.1039/x0xx00000x

1 significant role that is superior to patterned matrix in cell
2 alignment regulation.¹⁰⁻¹⁴ But with these physical features, a
3 continuous cell monolayer instead of hollow cell patterns is
4 usually obtained.¹⁵⁻¹⁷ Alternative solutions have been
5 developed by depositing smooth muscle cells on the inner
6 surfaces of orthogonally microtextured hollow tubes. But it is
7 difficult to precisely control the dimensions and shapes of these
8 hollow structures,¹⁸⁻²¹ which restricts their applications in
9 tissue engineering. In addition, skeletal muscle cells are
10 seldom studied on circular microtextured substrates or
11 tubes stated above because unlike circular smooth muscle
12 layers, most of circular skeletal muscle in vivo are macroscopic
13 structures except urethral sphincter whose diameter is about
14 two millimetres as minimum.
15 In this paper, we aimed to engineer circular and elliptical ring-
16 shaped cell patterns and maximize cell alignment
17 corresponded to cell patterns for urethral sphincter
18 engineering. In this scenario, dimension and curvature of
19 circular constraints should be taken into consideration.
20 Although myoblast behaviours under the influences of circular
21 ring-shaped matrix have been investigated, the width of the
22 pattern was fixed.^{22,23} Moreover, cells exhibit intrinsic chirality
23 on patterned matrix with circular boundaries which block
24 end-to-end cellular sequence with respect to circular
25 pattern.^{22,24} Cells are badly oriented and circular myotubes
26 can be hardly formed under this situation. Additionally,
27 considering the shape of urethral sphincter in vivo is more like
28 an elliptical than a circular ring, myoblast alignment under the
29 influence of parallelism of the inner and outer boundaries
30 constraint, which has not been considered in previous works
31 where constraints with parallel boundaries are used,^{18,22}
32 should also be investigated. For these purposes, glass
33 substrates patterned with concentric circular (parallel) and
34 elliptical (unparallel) polymeric microridges were presented.
35 These substrates were designed to pattern cells and maximize
36 cell alignment through combining the advantages of
37 mechanical and topological cues in cellular organization
38 regulation.
39 We find that dimension and parallelism other than curvature
40 of curved constraints profoundly affects myoblasts alignment.
41 To access the underlying mechanism of our experimental data,
42 we also proposed finite element models and implemented
43 drug test and hence revealed the role intercellular forces play
44 in cell alignment modulation. Myoblasts tend to align with the
45 direction of maximum intercellular principal stress exerted by
46 adjacent cells. The process can be strengthened by parallel
47 while disturbed by unparallel boundaries of constraint. With
48 these models, we also demonstrated why dimensions of
49 constraints can substantially affect cell alignment while
50 curvature of constraints cannot and why cells exhibit position-
51 dependent orientation behaviour with respect to boundaries
52 of constraint. Additionally, parallelism and dimension of
53 constraints also affect the differentiation of myotubes through
54 altering the shape of myoblasts and their nuclei. Due to the
55 simplicity of fabrication, our substrate provide an effective
56 method to maximize curved myoblast alignment for circular
57 myotubes generation towards sphincter tissue engineering.

Materials and Methods

Substrate fabrication

Substrates were fabricated by standard photolithography procedures. Briefly, coverslips (Citoglas, China), 20 mm × 20 mm × 0.17 mm, were pre-cleaned and dried before used. Then Hexamethyldisilazane (HMDS, Sigma Aldrich, US) was spin coated on coverslips as adhesive layer. AR-P3540T photoresist (Allresist GmbH, Germany) was spin coated, exposed with a mask under UV radiation for 10 s, developed in AR-P200 and then baked at 120 °C for 20 min. Substrates were then plated into 35 mm petri dishes, sterilized and coated with 6 μg ml⁻¹ collagen rat tail, type I solution (Gibco, US) and sterilized again before used. Atomic force microscopy (AFM) were used to measure the thickness of coated collagen layer and the stiffness (Young's Modulus) of the substrates.

Cell culture

C2C12 mouse myoblast cell line (Cell Bank of Chinese Academy of Sciences, China) were cultured in Dulbecco's Modified Eagle Medium supplemented with 10% fetal bovine serum and 1% streptomycin/penicillin (Culture medium, Gibco, US) and incubated at 5% CO₂, 37 °C. Cells were trypsinized, centrifuged and resuspended with fresh culture media after confluent. Afterwards, cells were seeded on substrates at 2 × 10³ cells cm⁻² and incubated. Cells were examined at 16, 24, 44 and 51 h after culture.

To further probe the effect of cell-cell contacts in cell alignment regulation, cells were treated with 20 μM blebbistatin (Sigma Aldrich, US) to partially inhibit cell-cell adhesion junctions. Blebbistatin were prepared in dimethyl sulfoxide (Thermo Fisher Scientific, US) and diluted with culture medium. The drug treated cells were incubated for 4 h prior to analysis to ensure the effect of inhibition.

Fluorescent staining

Cells nuclei and F-actin were stained with DAPI (Sigma Aldrich, US) and Rhodamine Phalloidin (Invitrogen, US) in dark room respectively. Briefly, Cell culture media was removed and 4% formaldehyde (Invitrogen, US) was added to petri dishes at room temperature for 15 min to fix cells. Then cells were permeated with 0.5% Triton X-100 solution (Invitrogen, US) at room temperature for another 15 min. Afterwards cells were blocked with 3% BSA (Invitrogen, US) at room temperature for 1 h. Cells were then stained with 5 μg ml⁻¹ Rhodamine Phalloidin (Molecular Probes, US) and incubated for 1 h at room temperature for F-actin. Afterwards, cells were stained with 300 nM 4', 6-diamidino-2-phenylindole (Molecular Probes, US) for 5 min at room temperature and mounted for imaging.

Cell shape and alignment

Quantitatively analysis was implemented by outlining the contour of every identifiable cell manually using Fiji/ImageJ (National Institutes of Health, US). For an individual cell, cell aspect ratio was used to characterize cell shape. Cell aspect ratio is defined as the ration of cell length to cell width (defined by the length of long and short axes of cellular best fit ellipse respectively). Cell center was defined as the center of

1 the ellipse. Groove direction was defined as the tangent
2 direction of the point on groove sidewalls that was nearest
3 cell center. Cell alignment angle was calculated as the angle
4 between cellular long axis and groove direction.

5 Modelling of mechanical stress of patterned cell sheets

6 Mechanical stress distribution of patterned cell sheet was
7 analysed by finite element method.^{23, 25, 26} The circular and
8 elliptical ring-shaped finite element model consists of a 5 μm
9 thick contractile top layer to simulate cell layer and a 1 μm
10 thick passive bottom layer with a fixed bottom surface to
11 simulate extracellular matrix layer. Other dimensions of the
12 model were prescribed elsewhere. A thermal strain induced by
13 dropping the temperature by 5 K on top layer was imported to
14 simulate cell contraction. The thermal conductivity and
15 coefficient of expansion of top layer were defined as 10 W m⁻¹
16 K⁻¹ and 0.05 K⁻¹ respectively. Both the top and the bottom
17 layers were treated as isotropic elastic material with value of
18 0.499 for the Poisson's ratio and 500 and 100 Pa for the
19 Young's Modulus respectively. The elemental maximum
20 principal stress of top layer was reported as maximum
21 intercellular principal stress. Meshes of different sizes (varied
22 from 1-10 μm) were generated to confirm the convergence
23 of the result.

24 Data processing and statistical analysis

25 All images were taken with Leica DMI3000B (Leica, Germany)
26 microscope using phase contrast and fluorescent mode and
27 processed with MATLAB (MathWorks, US) and Fiji/ImageJ
28 image processing software and associated plugins (National
29 Institutes of Health, US). Three randomly chosen regions for
30 each substrate were imaged. One-way analysis of variance
31 (ANOVA) followed by Turkey's post-hoc analysis for pairwise
32 means comparisons was performed to determine the
33 statistically differences between or within each group unless
34 otherwise mentioned. The statistical significance was defined
35 as * $p < 0.05$, ** $p < 0.01$, *** $p < 0.005$. Statistical analysis was
36 implemented with and statistical graphs were drawn by Origin
37 (OriginLab, US).

38 Results

39 Photolithography fabricated ring-shaped composite polymer and 40 glass substrates

41 Concentric circular and elliptical groove patterned substrates
42 were fabricated by standard photolithography procedures (Fig.
43 1A-D). Circular substrates consist of 100, 150 and 200 μm wide
44 grooves spacing 100, 150 and 200 μm apart respectively.
45 Elliptical substrates consist of 50 to 100, 75 to 150 and 100 to
46 200 μm wide grooves spacing 50, 75 and 100 μm apart in short
47 axis direction and 100, 150 and 200 μm apart in long axis
48 direction respectively (Fig. 1E-H). Both circular and elliptical
49 substrates were fabricated with two groove depths of 1.7 and
50 0.4 μm . All cells were cultured on substrates with 1.7 μm deep
51 grooves with flat substrate as control unless otherwise
52 mentioned. Cellular morphological and alignment parameters
53 are illustrated in Fig. 11.

54 Cell distribution on ring-shaped composite substrates

Distributions of cells cultured on concentric circular and
elliptical patterned substrates were characterized by showing
the number of cells proliferated in grooves as a percentage of
total cells (G for short). Cells crossing groove sidewalls were
defined as cells on ridges (Fig. 2A). On circular substrates, cells
showed a clearly preference for proliferating in grooves.
Percentages of cells in grooves of substrates with all
dimensions increased and reached their maximum after 44 h
of culture (G = 0.88 \pm 0.07, 0.95 \pm 0.07 and 0.83 \pm 0.02 for 100,
150 and 200 μm substrates respectively) (Fig. 2B). Cells were
separated and formed several circular patterns, no closed
pattern though, with regard to substrate patterns (Fig. 2). Then
percentage of cells in grooves decreased but no significant
difference occurred at 51 h of culture. On elliptical substrates,
cells distribution exhibited similar trends (Fig. 2B). The turning
point of percentage of cells in 150 and 200 μm wide grooves
occurred at 44 h of culture while percentage of cells in 100 μm
wide grooves began to decrease at 24 h of culture. No
statistically significant difference was found among all groove
dimensions at each examine time point ($p > 0.1$ for all cases).

Cell alignment on ring-shaped composite substrates

With previous definitions (Fig. 11), cell alignment angle (θ) can
be calculated as

$$\theta = \begin{cases} |\alpha - \beta|, & \text{if } |\alpha - \beta| \leq 90^\circ \\ 180^\circ - |\alpha - \beta|, & \text{else} \end{cases}$$

With the purpose of obtaining hollow cell patterns with well
oriented cells, we only focused on cells that were proliferated
in grooves. Cell alignment degree (D) was calculated by using
the average value of second order Legendre polynomial of cell
alignment angle (θ), an approach commonly employed when
characterizing the preferred directionality in liquid crystals.<sup>27,
28</sup>

$$D = \left\langle \frac{3\cos^2\theta - 1}{2} \right\rangle$$

D will approach 1 if θ approach 0 degree, which means there is
a strong degree of correlation between cell angle and groove
direction. D will approach 0 if θ is randomly distributed, which
means cells are randomly oriented. Moreover, D will approach
-0.5 if θ approach 90 degree, which means cells orient
perpendicular to groove direction (Fig. 2C). On circular
substrates, cell alignment degree increased from cell seeding
to 44 h after cell culture for 100 and 150 μm substrates (Fig.
2D). After 51 h of culture, alignment degree of cell in 100 (D =
0.86 \pm 0.05) and 150 μm (D = 0.78 \pm 0.06) wide grooves were
significantly higher than that of cells in 200 μm wide grooves
(D = 0.63 \pm 0.03) ($p < 0.005$ in both cases). For cells proliferated
on concentric elliptical patterned substrates, alignment degree
of cells in 100 μm wide grooves (D = 0.90 \pm 0.03) was found
significantly higher than that of cells in 150 and 200 μm wide
grooves after 51 h of culture. (D = 0.57 \pm 0.2 and 0.55 \pm 0.12, p
= 0.048 and 0.044 respectively). In addition, cell alignment
angles were more concentrated for cell on all substrates at 51
h of culture because standard deviations of cell alignment
degree decreased as culture time increased (Fig. 2D).

In order to study the influence of curvature on cell alignment,
we examined cell alignment degree on concentric circular

1 patterned substrates. Each ring-shaped groove composes two
 2 circular sidewalls with different radii. For an individual cell that
 3 proliferates in such a groove, cell alignment is supposed to be
 4 more closely affected by one groove sidewall if that wall is
 5 nearer to cell center than the other one. Thus cells proliferated
 6 on certain substrate can be divided into several groups, each
 7 characterized by one radius of curvature (R_c) of groove
 8 sidewalls (Fig. 3A-B and Fig. S1). Generally, relative frequency
 9 declined as cell alignment angle increased for all curvatures
 10 (Fig. 3C-E.). One-way ANOVA of cell alignment degree of
 11 different groove curvatures showed no significant difference
 12 when groove widths are 100 and 150 μm (Fig. 3F, $p = 0.66$ and
 13 0.23 respectively). For 200 μm substrate, pairwise comparison
 14 of cell alignment degree of different groove curvatures
 15 showed no significant difference ($p > 0.33$ for all cases) except
 16 when alignment degree of the groove curvature whose R_c is
 17 300 μm is compared to those whose R_c are 500 and 700 μm
 18 (Fig. 3E-F, $p = 0.016$ and 0.048 respectively).
 19 Cell alignment degree of circular and corresponding elliptical
 20 substrates were also compared to evaluate the influence of
 21 parallelism of constraints boundaries on cell orientation. There
 22 was no statistically difference of cell alignment degree
 23 between parallel and unparallel constraints (Fig. 4A-B).
 24 **Cell and nuclear shape on ring-shaped composite substrates**
 25 Cell and nuclear aspect ratio were used to characterize their
 26 shape. By 51 h time point, cell aspect ratio was significantly
 27 higher on 100 μm substrates than on 150 and 200 μm
 28 substrates (Fig. S2, $p < 0.005$ for both cases). At the same time,
 29 cell aspect ratio was independent of the curvatures of
 30 constraints (Fig. 4C). Moreover, there was no statistically
 31 difference of cell aspect ratio between circular and
 32 corresponding elliptical substrates with parallel and unparallel
 33 boundaries respectively (Fig. 4D). Although nuclear aspect
 34 ratio were higher on patterned composite substrates than on
 35 flat glass substrate, there was no statistically difference of that
 36 between all circular and corresponding elliptical substrates
 37 and between all circular and elliptical substrates with different
 38 dimensions. However, the significant level of circular and
 39 corresponding elliptical substrates compared to flat substrate
 40 differs. Nuclei on circular substrates elongated more
 41 significantly than on corresponding elliptical substrates (Fig. S3).

42 **Discussions**

43 **Distribution of myoblasts is a result of complex cellular response**
 44 **to combinational guidance features**

45 It has been proved that stiffness is a strong tool to pattern cells
 46 even superior to patterned matrix.¹⁰ Spatial stiffness variations
 47 can induce durotaxis and form cell patterns.²⁹ Here, the
 48 stiffness difference of polymeric ridges and glass grooves could
 49 lead myoblasts to migration towards stiff grooves other than
 50 soft ridges. Moreover, cells can sense the effective stiffness of
 51 rigid substrates that are not in direct cellular contact when
 52 they are cultured on a thin polymeric film affixed to a rigid
 53 substrate.³⁰⁻³³ Therefore we could expect that myoblasts were
 54 randomly distributed when polymeric film was thin enough so

that myoblasts were unable to sense the difference of the
 effective stiffness between ridge and groove surfaces because
 stiffness of glass could be transferred to ridge surface. To test
 our hypothesis, we first confirmed that the collagen was
 uniformly coated on glass and photoresist with the same
 thickness. Then we performed nanoindentation on the surface
 of collagen coated glass, 0.4 μm and 1.7 μm thick photoresist
 on glass respectively. The results showed that 0.4 μm
 photoresist is as stiff as glass while stiffer than 1.7 μm
 photoresist (Fig. S6). Afterwards, we cultured myoblasts on
 substrates with the same patterns but 400 nm deep grooves.
 No cell pattern was formed and no organization was observed
 as expected even at 72 h after culture (Fig. S3). To exclude a
 mere effect of substrate grooved pattern on cell distribution,
 we cultured cells on grooved glass substrate (without polymer)
 with the same pattern and groove depth (1.7 μm) as the
 composite substrate previously presented. Myoblasts showed
 no preference for going inside and proliferating in the grooves
 after 72 h of culture (Fig. S4). To further exclude the effect of
 collagen, we cultured cells on collagen coated and non-coated
 substrates. Although cells were more elongated on collagen
 coated than non-coated substrates, similar distribution were
 formed on both substrates (Fig. S5). Therefore, we confirmed
 that stiffness played an important role in cell distribution
 because no material surface properties varies but effective
 stiffness as polymer film thinning. Additionally, cells located on
 plateau ridges were less elongated and more spread than
 those located in grooves (Fig. 5A). This infers that the
 difference of surface chemistry between grooves and ridges
 also might contribute to cells distribution through forming
 different collagen crosslinking density. These cues indicate that
 the distribution of myoblasts could be a result of complex
 cellular response to combinational guidance features.

Effects of ring-shaped composite substrates on cell alignment

Curvature of curved constraint has no influence on cell alignment. It is found that cell-cell interaction acts as the
 communication pathway for passing microenvironment
 information between neighbouring cells to induce the
 direction of cell growth and migration.³⁴⁻³⁶ Therefore cell
 contact guidance can be induced not only by subcellular scale
 constraints, but also by supracellular scale constraints as well.
 In addition, the diameter of the muscle layer of hollow tissues
 and organs in vivo varied from microns to centimetres.
 Recently, influence of supracellular scale curvature on cell
 mechanics was studied on the surface of cylinders or on the
 inner surface of tubular structures.^{2, 37-39} But the influence of
 curvature on myoblast alignment has not been quantitatively
 elucidated. In this paper we cultured myoblasts on both
 concentric circular and elliptical substrates. To get rid of the
 influence of groove width, we mostly focused on cell
 alignment of concentric circular substrate that composes
 grooves with a fixed width but varied curvatures. Statistical
 analysis demonstrated that curvatures had no significant
 influence on cell alignment for 100 and 150 μm substrates,
 which means curved constraints can also induce contact
 guidance effectively (Fig. 3F). As for 200 μm substrate, it is

1 worth noting that pairwise comparison of cell alignment 58
 2 degree of all radii of curvatures higher and lower than 300 μm 59
 3 showed no significant influence on cell alignment ($p = 0.46$) 60
 4 Therefore we believe the significant decline of cell alignment 61
 5 degree at 300 μm was caused by the lack of cell-cell contact 62
 6 some local regions near groove sidewall which led 63
 7 insufficient cell-cell interactions to pass the boundary 64
 8 information of constraints to the neighbouring cells. Overall 65
 9 the results suggest that myoblasts can orient along curved 66
 10 constraints independent of their curvatures. 67
 11 **Dimension of curved constraint significantly affects cell 68**
 12 **alignment.** Although the effects of groove width on myoblast 69
 13 alignment, morphology and differentiation have been 70
 14 investigated substantially, few studies have investigated the 71
 15 role which width plays in curved constraints. Recent 72
 16 osteoblasts were observed to orient along groove direction 73
 17 when cultured on concentric circular grooves with width w 74
 18 below 100 μm . Percentages of cell alignment angle smaller 75
 19 than 15 degrees decreased from 75% to 20% when groove 76
 20 width increased from 7.5 to 96.2 μm .⁴⁰ On the contrary 77
 21 myoblasts were highly oriented along groove direction 78
 22 substrates with groove width beyond 100 μm here which is 79
 23 favour of tissue scaffold fabrication because mesoscale 80
 24 features can be fabricated more easily. In addition, cell-cell 81
 25 contacts weakened as groove width increased because more 82
 26 space are available for cells to proliferate and migrate, which 83
 27 responsible for the phenomenon that better oriented cells 84
 28 were observed in narrower grooves in our experiment (Fig. 85
 29 2D). 86
 30 **Parallelism of boundaries of curved constraint significantly 87**
 31 **affects cell alignment.** Concentric circular substrate can serve 88
 32 as the control group of elliptical substrate because cell 89
 33 alignment is not affected by mechanical constraints curvature 90
 34 as we demonstrated, consistent with previous study that align 91
 35 myoblasts on matrix constraints.²³ Since substrate dimension 92
 36 instead of curvature significantly affect cell alignment as stated 93
 37 above, it is expected that cells were better oriented along 94
 38 groove directions on elliptical substrates because groove 95
 39 widths of the 100, 150 and 200 μm patterned substrates 96
 40 actually vary from 50 to 100 μm , 75 to 150 μm and 100 to 200 97
 41 μm respectively. However, there was no statistically significant 98
 42 difference of cell alignment degree between circular and 99
 43 corresponding elliptical substrates ($p > 0.1$ for all cases) (Fig. 100
 44 2D). It is worth noting that concentric elliptical grooves here 101
 45 presented do not possess parallel elliptical groove sidewall 102
 46 indeed (Fig. S7). Therefore, these results infer that parallelism 103
 47 of constraint also plays an important role in cell alignment 104
 48 regulation. Constraint with parallel boundaries can favour 105
 49 align cells with boundaries directions, thus resulting in higher 106
 50 cell alignment degree than constraint with unparallel 107
 51 boundaries. 108
 52 **The mechanisms underlying the influences of dimension, 109**
 53 **curvatures and parallelism of boundaries of constraint on cell 110**
 54 **alignment.** We observed that before cells filled the surface 111
 55 the grooves, cells exhibited low degree of alignment. Only cells 112
 56 proliferated near groove sidewalls oriented along groove 113
 57 directions and cells proliferated in the middle region of 114

grooves were random aligned. However, when cells sufficiently
 filled the surface of the grooves, which led to high level cell-
 cell contacts, they started to realign along grooves directions
 (Fig. S8). It has been proved that cell-cell contacts can transmit
 intercellular normal and shear stresses and eventually align
 the long axis of the cell along the orientation of local minimal
 intercellular shear stress, which equivalents to the orientation
 of maximum principal stress.^{35,41} Therefore, we assumed that
 the orientation of maximum intercellular principal stress
 depends not on curvatures but on dimensions and parallelism
 of curved constraint. To test our hypothesis, we inspected the
 orientation of maximum intercellular principal stress exerted
 by adjacent cells under the influence of curved parallel and
 unparallel constraints with varied dimensions and curvatures.
 Finite element analysis was implemented to evaluate the bias
 angle (θ_s) of orientation of maximum principal stress with
 respect to constraint directions (Fig. 6).

To assess the mechanisms underlying the influence of
 dimension and curvature of circular ring-shaped constraints on
 cell alignment, we built circular ring-shaped finite element
 models with a fixed inner diameter and varied distances
 between the inner and outer boundaries and with varied inner
 diameters and a fixed distance of 150 μm between the inner
 and outer boundaries, respectively. Other details of the
 models have been prescribed above. We found that θ_s
 enlarges significantly as the distance between the inner and
 outer boundaries increases ($p < 0.001$, Fig. 6C). This result
 reconfirms our experimental results which concluded
 myoblasts orient along directions of boundaries better in
 narrower constraints than in wider ones and reveals that
 intercellular stresses are the driven forces that align myoblast
 along curved constraints. Additionally, the deviation of θ_s also
 extends as width of constraint increases. The color-coded
 orientation maps in Fig. 6C shows that θ_s enlarges as the
 distance between meshed elements that simulates cells and
 boundaries of constraint increases and reaches its maximum in
 the middle regions between inner and outer boundaries of
 constraint with a given width. Previous studies have observed
 that cell alignment with respect to direction of constraint
 boundary depends on cellular distance from the boundaries.^{42,}
⁴³ Our result provides this phenomenon a theoretical
 interpretation and emphasizes the vital role that intercellular
 forces play in inducing cell alignment.

To explore the mechanisms underlying the influence of
 curvature of circular ring-shaped constraints on cell
 orientation, we fixed widths of ring-shaped constraints at 150
 μm while decreased curvatures of boundaries of constraints.
 We found homogeneous patterns of color-coded maps of θ_s
 regardless of increasing radii of both boundaries ($p > 0.1$, Fig.
 6D). This indicates that orientation of maximum intercellular
 principal stress, which equivalent to cell orientation as stated
 above, is independent of curvature of curved constraints,
 consistent with our experimental results.

We then explored the influence of parallelism on θ_s . To
 simplify the model but not loss generality, we built an
 unparallel elliptical ring-shaped finite element model with
 corresponding parallel elliptical model as control. The in plane

1 dimensions of the parallel and unparallel models were 58
2 described above. Although width of unparallel model is small 59
3 than that of parallel model, the finite element result of 60
4 showed no significant difference ($p > 0.1$, Fig. 6E). The 61
5 simulation results are in conflict with our previous conclusion 62
6 depicting that narrow curved constraints are superior to wide 63
7 ones. Instead, it demonstrates the role that parallelism 64
8 boundaries of constraints plays in cell alignment guidance 65
9 which agrees with our experimental results. To verify that it is 66
10 unparallel boundaries of constraints that disorders orientation 67
11 of maximum principal stress, we also evaluated the degree 68
12 parallelism of elliptical ring-shaped constraint through 69
13 calculate the angle (θ_p) between the direction of inner and 70
14 outer boundaries with respect to locations across the entire 71
15 constraint (Fig. 6B). We found that the most unparallel regions 72
16 between inner and outer boundaries locate around both ends 73
17 of long axis, consistent with the locations of the most 74
18 disordered orientation of maximum principal stress in our 75
19 finite analysis results. The same scenario appears at regions 76
20 near both ends of short axis, where highly ordered maximum 77
21 principal stress was observed with parallel boundaries (Fig. 6F). 78
22 These results infer that there is a strong correlation 79
23 between parallelism of boundaries of constraint and cell 80
24 orientation. Constraints possessing parallel boundaries are 81
25 more conducive to inducing cell alignment, providing guidance 82
26 in the design of scaffolds for noncircular hollow tissues 83
27 engineering. 84
28 To confirm the relationship of cell alignment with respect 85
29 cooperative intercellular forces, we performed an drug test 86
30 experiment to partially inhibit cell-cell connections through 87
31 treating high level contacted cells with 20 μM blebbistatin.^{44, 45} 88
32 Cell alignment angle with respect to groove direction was 89
33 calculated. The results showed that cells were highly aligned 90
34 along groove directions with over 70% cells aligned within 20 91
35 degrees of groove directions before drug treatment for both 92
36 circular and elliptical substrates. However, cells began 93
37 randomly oriented which resulted in the same parameter 94
38 mentioned dropped to under 40% when cell-cell connections 95
39 were inhibited (Fig. 7). 96
40 Taken our experimental, simulation and drug test results 97
41 together, we can conclude that cooperative intercellular forces 98
42 exerted by adjacent cells are the driving forces that propel 99
43 cells to reoriented themselves to align along the directions of 100
44 boundaries of curved constraint. By combining the effects of 101
45 the topographic, mechanical and surface chemistry properties 102
46 of boundaries on cell organization, our substrates eliminated 103
47 the impeditive effect cell chirality excreted on the formation 104
48 end-to-end cellular sequence with respect to cell pattern when 105
49 cells were seeded on patterned matrix. 106
50 Although glass is not an implantable material, our model 107
51 showed that the mechanisms of how dimension, curvature and 108
52 parallelism affect cellular organization are basically 109
53 independent of the materials of substrate. The model only set 110
54 line for stiffness of the material so that cells cannot 111
55 substantially deform the substrate. Materials satisfying the 112
56 condition, whether they are porous, biocompatible and 113
57 biodegradable or not, can utilize our model. Therefore, we

believe that design rules derived from the in vitro studies reported here can be applied when designing scaffolds utilizing implantable materials to improve sphincter-like tissue regeneration strategies in vivo.

Effects of ring-shaped composite substrates on myoblast shape

The altered cell and nuclear shape play an important role in the differentiation of myotubes.^{46, 47} Based on our observations that cells were more elongated in circular narrow constraints than in wide ones and that curvature showed no influence on cell aspect ratio, we can preliminary count that substrate dimension dominates cell aspect ratio. However, there was no statistically difference of cell aspect ratio between circular and corresponding elliptical substrates whose dimensions are narrower than circular ones expect 100 μm substrates (Fig. 4D). Therefore we can conclude that parallelism of constraint boundaries also significantly affects cell aspect ratio. Additionally, cytoplasmic actin filaments are essential features in the modulation of nuclear shape and function. It has been proved that there exists a mechanistic coordination between cell and nuclear shape.^{48, 49} Consequently, nuclear aspect ratio obey the same rules set by dimension and parallelism of constraint for cell aspect ratio.

Conclusions

This study revealed a simple way to engineer circular and elliptical ring-shaped myoblast patterns and maximize corresponding cell alignment simultaneously. Different from previous methods that pattern cells with patterned matrices and stiffness fabricated through microcontact printing and soft lithography, the method presented is mold-free. We demonstrated that myoblasts are able to orient along our substrates with width of several folds beyond typical individual cell scale even when the constraints is curved. This result is important because it means that we can engineer large-scale ring-shaped tissue in a cheap way since supracellular scale constraints can be fabricated easier than subcellular ones. We also proved, both experimentally and theoretically, that myoblasts track direction of curved constraints better in narrower constraints than in wider ones. Therefore, compromises should be made between the degree of cell alignment and the cost of the fabrication of scaffolds when we design the dimensions of scaffolds. Interestingly, as a typical character of curved constraints, curvature showed no influence on myoblasts alignment. Additionally, we also investigated the influence of parallelism of the constraints on cell behaviour and demonstrated that constraints with parallel boundaries are prone to induce contact guidance better than unparallel ones. To the best of our knowledge, this is the first time that influence of parallelism of constraints on cells behaviour is investigated. In fact, parallelism of curved constraint is one character that we cannot disregard in the design of the substrate or scaffold for noncircular ring-shaped tissue engineering. We concluded that narrow and parallel features are key parameters that should be considered in the design of curved constraints in order to maximize cell

- 1 alignment for ring-shaped myotubes generation. These design 56 17. C. L. Gilchrist, D. S. Ruch, D. Little and F. Guilak, *Biomaterials*, 2014, **35**, 10015-10024.
- 2 rules can be incorporated into the surface of scaffolds utilizing 57 18. Y. M. Wang, H. G. Shi, J. Qiao, Y. Tian, M. Wu, W. Zhang, Y.
- 3 implantable materials for urethral sphincter engineering. 58 Lin, Z. W. Niu and Y. Huang, *ACS Appl. Mater. Interfaces*,
- 4 Finally, although rigid materials such as glass are not ideal 59 2014, **6**, 2958-2962.
- 5 candidates for optimal myotubes differentiation, on 60 19. B. Yuan, Y. Jin, Y. Sun, D. Wang, J. S. Sun, Z. Wang, W.
- 6 substrates hold the potential to server as a compliant bottom 61 Zhang and X. Y. Jiang, *Adv. Mater.*, 2012, **24**, 890+.
- 7 layer of glass-attached myotubes with tissue like stiffness for 62 20. J. S. Choi, Y. Piao and T. S. Seo, *Biomaterials*, 2014, **35**, 63-
- 8 cell-on-cell sphincter-like tissue engineering,^{50, 51} which can 63 70.
- 9 potentially benefit the treatment of stress urinary 64 21. M. T. McClendon and S. I. Stupp, *Biomaterials*, 2012, **33**,
- 10 incontinence. 65 5713-5722.
- 66 22. L. Q. Wan, K. Ronaldson, M. Park, G. Taylor, Y. Zhang, J. M.
- 67 Gimble and G. Vunjak-Novakovic, *Proc Natl Acad Sci U S A*,
- 68 2011, **108**, 12295-12300.
- 11 **Acknowledgements** 69 23. P. Bajaj, B. Reddy, L. Millet, C. N. Wei, P. Zorlutuna, G. Bao
- 12 We appreciate Dr. Zhen Guo and the Laboratory of Cellular 70 and R. Bashir, *Integr. Biol.*, 2011, **3**, 897-909.
- 13 Dynamics at University of Science and Technology of China for 71 24. Y. H. Tee, T. Shemesh, V. Thiagarajan, R. F. Hariadi, K. L.
- 14 their kindly support. 72 Anderson, C. Page, N. Volkmann, D. Hanein, S.
- 73 Sivaramakrishnan, M. M. Kozlov and A. D. Bershadsky,
- 74 *Nat. Cell Biol.*, 2015, **17**, 445+.
- 15 **References** 75 25. C. M. Nelson, R. P. Jean, J. L. Tan, W. F. Liu, N. J. Sniadecki,
- 16 1. A. Stenzl and K. D. Sievert, *European urology*, 2007, 76 A. A. Spector and C. S. Chen, *Proc. Natl. Acad. Sci. U. S. A.*,
- 17 1574-1575. 77 2005, **102**, 11594-11599.
- 18 2. F. A. Zouraq, M. Stölting and D. Eberli, *Skeletal Muscle* 78 26. B. Li, F. Li, K. M. Puskar and J. H. Wang, *J Biomech*, 2009,
- 19 *Regeneration for Clinical Application*, 2013. 79 **42**, 1622-1627.
- 20 3. Y. Shi, Y. Li, J. Liu and Y. Zhang, *Cell Therapy and Muscle* 80 27. A. Leclerc, D. Tremblay, S. Hadjiantoniou, N. V.
- 21 *Regeneration: Skeletal Myogenic Differentiation of Urine* 81 Bukoreshtliev, J. L. Rogowski, M. Godin and A. E. Pelling,
- 22 *Derived Stem Cells for Potential Use in Treatment of* 82 *Biomaterials*, 2013, **34**, 8097-8104.
- 23 *Urinary Incontinence*, 2013. 83 28. W. F. Zheng and X. Y. Jiang, *Colloid Surface B*, 2014, **124**,
- 24 4. D. Huh, Y. S. Torisawa, G. A. Hamilton, H. J. Kim and D. 84 97-110.
- 25 Ingber, *Lab Chip*, 2012, **12**, 2156-2164. 85 29. T. H. Qazi, D. J. Mooney, M. Pumberger, S. Geissler and G.
- 26 5. F. Khan, M. Tanaka and S. R. Ahmad, *J Mater Chem B* 86 N. Duda, *Biomaterials*, 2015, **53**, 502-521.
- 27 2015, **3**, 8224-8249. 87 30. A. Higuchi, Q. D. Ling, S. S. Kumar, Y. Chang, A. A. Alarfaj,
- 28 6. M. Verhulsel, M. Vignes, S. Descroix, L. Malaquin, D. M. 88 M. A. Munusamy, K. Murugan, S. T. Hsu and A. Umezawa,
- 29 Vignjevic and J. L. Viovy, *Biomaterials*, 2014, **35**, 1816 89 *J Mater Chem B*, 2015, **3**, 8032-8058.
- 30 1832. 90 31. A. Buxboim, K. Rajagopal, A. E. X. Brown and D. E. Discher,
- 31 7. X. Yao, R. Peng and J. D. Ding, *Adv. Mater.*, 2013, 91 *J. Phys.-Condes. Matter*, 2010, **22**.
- 32 5257-5286. 92 32. B. Oommen and K. J. Van Vliet, *Thin Solid Films*, 2006,
- 33 8. C. A. DeForest and D. A. Tirrell, *Nat. Mater.*, 2015, 93 **513**, 235-242.
- 34 523-531. 94 33. I. T. Hoffecker, W. H. Guo and Y. L. Wang, *Lab Chip*, 2011,
- 35 9. M. V. Tsurkan, R. Wetzel, H. R. Perez-Hernandez, 95 **11**, 3538-3544.
- 36 Chwalek, A. Kozlova, U. Freudenberg, G. Kempermann, Y. 96 34. X. Trepat, M. R. Wasserman, T. E. Angelini, E. Millet, D. A.
- 37 Zhang, A. F. Lasagni and C. Werner, *Adv Healthc Mater* 97 Weitz, J. P. Butler and J. J. Fredberg, *Nat Phys*, 2009, **5**,
- 38 2014, DOI: 10.1002/adhm.201400395. 98 426-430.
- 39 10. Y. S. Choi, L. G. Vincent, A. R. Lee, K. C. Kretschmer, 99 35. D. T. Tambe, C. C. Hardin, T. E. Angelini, K. Rajendran, C. Y.
- 40 Chirasatitsin, M. K. Dobke and A. J. Engler, *Biomaterials* 100 Park, X. Serra-Picamal, E. H. H. Zhou, M. H. Zaman, J. P.
- 41 2012, **33**, 6943-6951. 101 Butler, D. A. Weitz, J. J. Fredberg and X. Trepat, *Nat.*
- 42 11. A. Higuchi, Q. D. Ling, Y. Chang, S. T. Hsu and A. Umezawa, 102 *Mater.*, 2011, **10**, 469-475.
- 43 *Chemical reviews*, 2013, **113**, 3297-3328. 103 36. S. R. K. Vedula, M. C. Leong, T. L. Lai, P. Hersen, A. J. Kabla,
- 44 12. J. L. Charest, M. T. Eliason, A. J. Garcia and W. P. King, 104 C. T. Lim and B. Ladoux, *Proc. Natl. Acad. Sci. U. S. A.*,
- 45 *Biomaterials*, 2006, **27**, 2487-2494. 105 2012, **109**, 12974-12979.
- 46 13. H. Y. Hsieh, G. Camci-Unal, T. W. Huang, R. Liao, T. J. 106 37. A. Y. Hsiao, T. Okitsu, H. Onoe, M. Kiyosawa, H. Teramae,
- 47 Chen, A. Paul, F. G. Tseng and A. Khademhosseini, *Lab* 107 S. Iwanaga, T. Kazama, T. Matsumoto and S. Takeuchi,
- 48 *Chip*, 2014, **14**, 482-493. 108 *PLoS One*, 2015, **10**, e0119010.
- 49 14. C. T. Ho, R. Z. Lin, R. J. Chen, C. K. Chin, S. E. Gong, H. Y. 109 38. H. Kang do, S. M. Kim, B. Lee, H. Yoon and K. Y. Suh, *The*
- 50 Chang, H. L. Peng, L. Hsu, T. R. Yew, S. F. Chang and C. H. 110 *Analyst*, 2013, **138**, 6230-6242.
- 51 Liu, *Lab Chip*, 2013, **13**, 3578-3587. 111 39. M. Junkin, S. L. Leung, S. Whitman, C. C. Gregorio and P. K.
- 52 15. A. M. Ross, Z. Jiang, M. Bastmeyer and J. Lahann, *Small* 112 Wong, *J. Cell Sci.*, 2011, **124**, 4213-4220.
- 53 2012, **8**, 336-355. 113 40. K. Wang, L. Cai, L. Zhang, J. Y. Dong and S. F. Wang, *Adv.*
- 54 16. L. Altomare, N. Gadegaard, L. Visai, M. C. Tanzi and S. 114 *Healthc. Mater.*, 2012, **1**, 292-301.
- 55 Fare, *Acta Biomater*, 2010, **6**, 1948-1957. 115 41. X. Trepat and J. J. Fredberg, *Trends Cell Biol.*, 2011, **21**,
- 116 638-646.
- 117

Paper

Journal of Materials Chemistry B

- 1 42. F. J. Segerer, F. Thuroff, A. P. Alberola, E. Frey and J. O.
2 Radler, *Phys. Rev. Lett.*, 2015, **114**, 5.
- 3 43. S. J. He, C. L. Liu, X. J. Li, S. P. Ma, B. Huo and B. H. Ji,
4 *Biophys. J.*, 2015, **109**, 489-500.
- 5 44. Z. Liu, J. L. Tan, D. M. Cohen, M. T. Yang, N. J. Sniadecki, S.
6 A. Ruiz, C. M. Nelson and C. S. Chen, *Proc Natl Acad Sci U*
7 *S A*, 2010, **107**, 9944-9949.
- 8 45. M. Vicente-Manzanares, X. F. Ma, R. S. Adelstein and A. R.
9 Horwitz, *Nat. Rev. Mol. Cell Biol.*, 2009, **10**, 778-790.
- 10 46. N. M. Rodríguez, R. A. Desai, B. Trappmann, B. M. Baker
11 and C. S. Chen, *Langmuir*, 2014, **30**, 1327-1335.
- 12 47. L. Wang, Y. Wu, B. Guo and P. X. Ma, *ACS Nano*, 2015, **9**,
13 9167-9179.
- 14 48. M. Versaevel, T. Grevesse and S. Gabriele, *Nature*
15 *communications*, 2012, **3**.
- 16 49. B. Chen, C. Co and C. C. Ho, *Biomaterials*, 2015, **67**, 129-
17 136.
- 18 50. A. J. Engler, M. A. Griffin, S. Sen, C. G. Bonnetmann, H. L.
19 Sweeney and D. E. Discher, *J. Cell Biol.*, 2004, **166**, 877-
20 887.
- 21 51. D. E. Discher, P. Janmey and Y. L. Wang, *Science*, 2005,
22 **310**, 1139-1143.

23

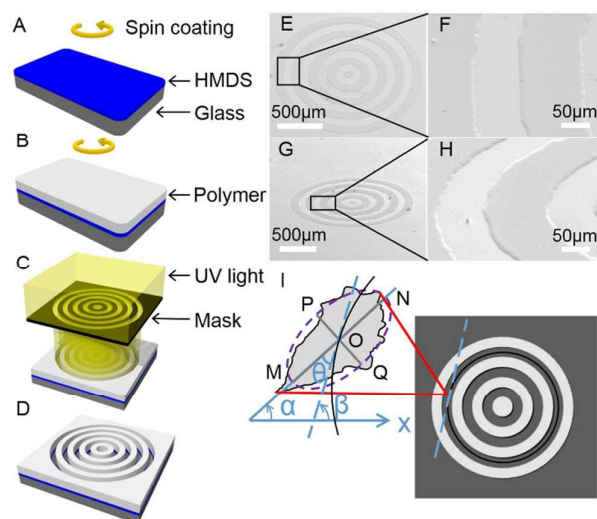


Fig. 1. Substrates fabrication and definition of cell shape and alignment. (A-D) Standard lithography procedures to fabricate substrate with circular and elliptical constraints. Linear constraints were drawn as example to illustrate the procedures. SEM images showed the fabricated circular (E-F) and elliptical (G-H) substrates with 150 μm wide concentric circular grooves spacing 150 μm apart. (I) Diagram illustrating cell aspect ratio and cell alignment angle (θ) on patterned substrate. The ellipse is the best fitted ellipse of cell shape. Angle of inclination of long axis and groove direction are represented by α and β respectively. Scale bar is 500 μm in (E) (G) and 50 μm in (F) (H).

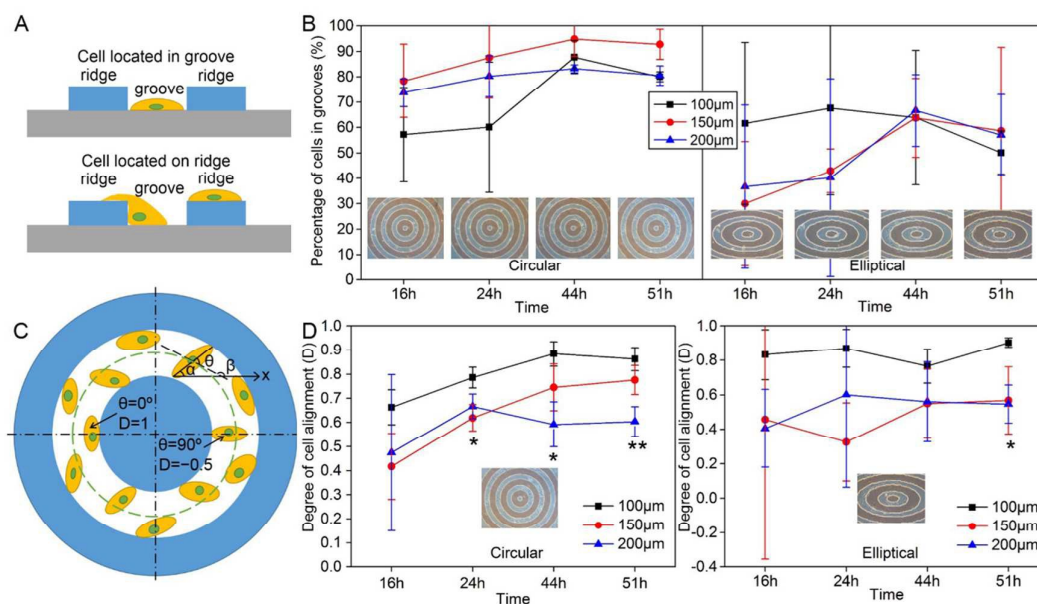


Fig. 2. Cell distribution and alignment on substrates patterned with curved constraints. (A) Diagram illustrating definition of cell located in groove or on ridge. (B) Percentage of cells located in grooves of concentric circular and elliptical patterned substrates as a function of time. Inset figures are phase contrast images at different time. (C) Diagram illustrating cell alignment angle and alignment degree. Cell angle and groove direction are shown as α and β . Cell alignment angle is shown as θ . (D) Alignment degree of cells in grooves of concentric circular and elliptical substrates as a function of time. All parameters were calculated and showed as mean \pm SD.

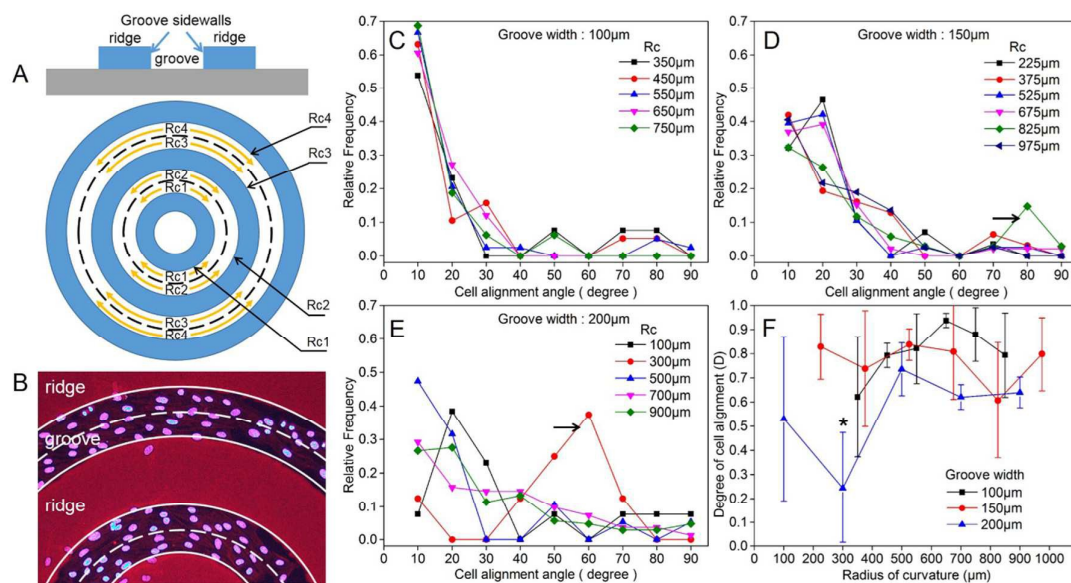


Fig. 3. Cell alignment angle distribution and cell alignment degree over radii of groove curvatures on circular patterned substrates at 51 h of culture. (A) Diagram illustrating groove sidewalls (top) and groove regions divided by the distance to groove sidewalls (bottom). Groove sidewalls were represented by radii of their curvatures from Rc1 to Rc4. Points on each dash line are equidistant from both groove sidewalls. Cells located in between Rc1 and dash line were supposed to be affected more by Rc1 and so on. (B) Fluorescent image of myoblasts nuclei (blue) and polymeric ridges (red) on 150 μm patterned substrate. Plots showed the distribution of cell alignment angle of different curvatures of grooves with widths of (C) 100 μm, (D) 150 μm and (E) 200 μm. (F) Degree of cell alignment (D) changed with groove curvatures on 100, 150 and 200 μm circular patterned substrates. If there is a high degree of parallel or perpendicular alignment between cell and groove direction, D will approach 1 or 0 respectively.

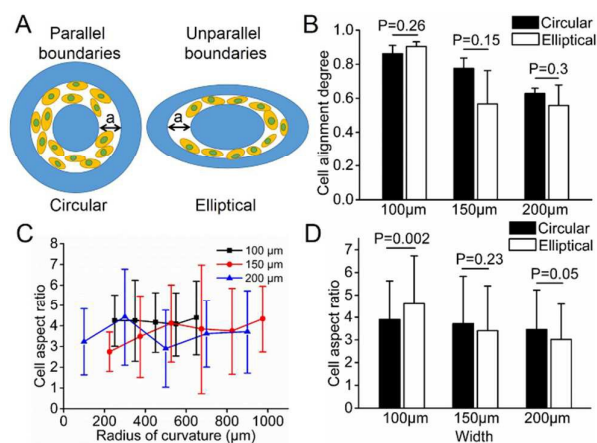


Fig. 4. Influence of parallelism of boundaries of constraints on cell alignment and cell aspect ratio. (A) Diagram illustrating constraints with parallel and unparallel boundaries. Parallel constraint provides fixed width while unparallel constraint provides varied width that is narrower than the former. Scale bars = 40 μm . (B) Comparisons of cell alignment degree between circular constraints with width of 100, 150 and 200 μm and corresponding elliptical constraints with width of 50 to 100, 75 to 150 and 100 to 200 μm . (C) Influence of curvature on cell aspect ratio. (D) Comparisons of cell aspect ratio between circular and elliptical constraints.

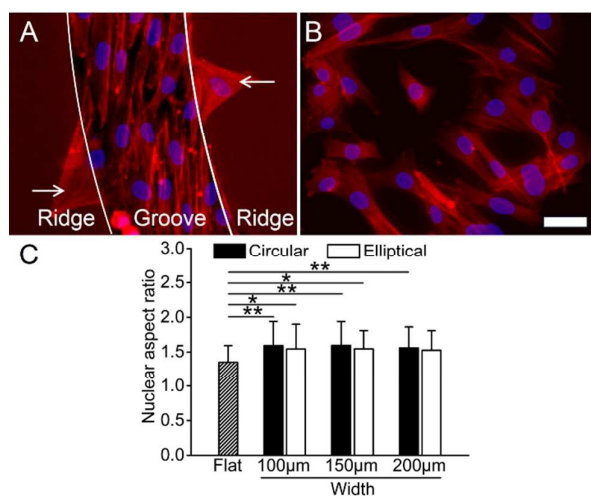


Fig. 5. Influence of substrate patterns on nuclear aspect ratio. (A) Fluorescent images of F-actin (red) and nuclei (blue) of cells on 150 μm circular composite and flat glass substrate (B) after 51 h of culture. Polymeric ridges were also imaged and showed in red. (C) Comparisons of nuclear aspect ratio of different substrate patterns.

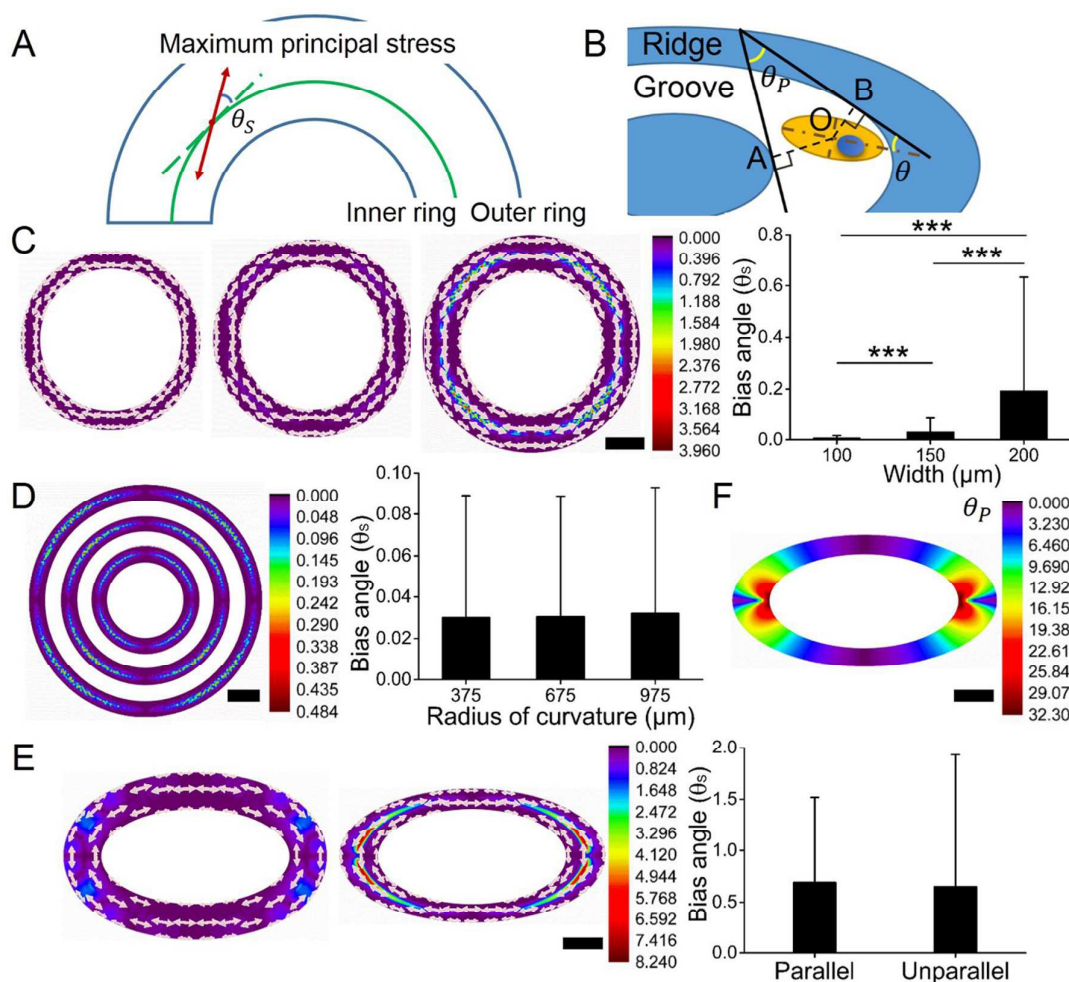


Fig. 6. Finite element results of orientation maps of intercellular maximum principal stresses with respect to directions of constraint boundary and parallelism maps of elliptical ring-shaped constraints with varied width (unparallel boundaries). Overlain upon these maps are white arrows depicting vectors of maximum principal stresses. (A) The bias angle of maximum principal stress (red line with arrows) was defined as θ_s based on the deviation from the circumferential direction (green dash line). (B) The degree of parallelism of inner and outer boundaries was defined as θ_p based on the interangle between tangent lines (black solid lines) of the nearest points on inner (point A) and outer (point B) boundaries with respect to cell center (point O). (C) Left panel shows color-coded maps of θ_s of circular ring-shaped models with inner diameter of 750 μm and a distance of 100 (left), 150 (middle) and 200 μm (right) between the inner and outer boundaries. Right panel shows θ_s of corresponding circular ring-shaped models with different width. (D) Left panel shows color-coded maps of θ_s of circular ring-shaped models with inner diameter of 750 (inner), 1350 (middle) and 1950 μm (outer) and a distance of 150 μm between the inner and outer boundaries. Right panel shows θ_s of corresponding models with different curvatures. (E) Left panel shows color-coded maps of θ_s of elliptical ring-shaped models with inner long and short axis of 750 and 375 μm and a distance of 150 μm between the inner and outer boundaries (left) and with inner ellipse the same dimensions as the inner ellipse of the former constraints and outer long and short axis of 1050 and 525 μm (right). Right panel shows θ_s of corresponding elliptical ring-shaped models with parallel and unparallel boundaries. Student t test was performed to determine the difference between the two groups. (F) Color-coded parallelism maps of θ_p of elliptical ring-shaped constraints. Scale bar is 200 μm in (C), (E) and (F) and 400 μm in (D).

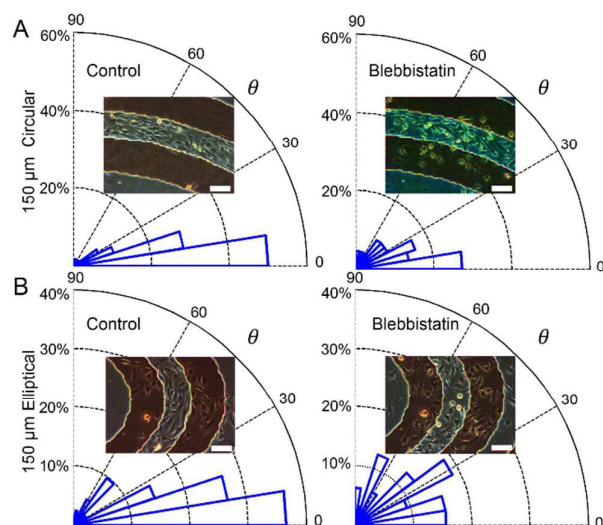


Fig. 7. Effect of blebbistatin induced cell-cell contact inhibition on cell alignment angle distribution. Alignment angle (θ) of cells on 150 μm circular (A) and elliptical (B) were calculated before and 4 h after blebbistatin treatment respectively. Insets were phase contrast images of cells at the same position of the substrate before and after drug treatment.

We introduce substrates of composite materials for sphincter tissue engineering and demonstrate the mechanisms of how dimension, curvature and parallelism of constraint affect cellular organization.

